



Research papers

A framework to improve hyper-resolution hydrological simulation in snow-affected regions



Xinyi Shen ^{*}, Emmanouil N. Anagnostou

Department of Civil and Environmental Engineering, University of Connecticut, Storrs, CT, United States

ARTICLE INFO

Article history:

Received 29 December 2016
 Received in revised form 9 May 2017
 Accepted 24 May 2017
 Available online 19 June 2017
 This manuscript was handled by Marco Borga, Editor-in-Chief

Keywords:

CREST
 Distributed hydrological model
 Snow process
 Hyper-resolution
 Flood

ABSTRACT

Snow processes in mid- and north-latitude basins and their interaction with runoff generation at hyper-resolution (<1 km and <hourly) pose challenges in current state-of-the-art distributed hydrological models. These models run typically at macro to moderate scales (>5 km), representing land surface processes based on simplified couplings of snow thermal physics and the water cycle in the soil-vegetation-atmosphere (SVA) layers. This paper evaluates a new hydrological model capable of simulating river flows for a range of basin scales (100 km² to >10,000 km²), and a particular focus on mid- and north-latitude regions. The new model combines the runoff generation and fully distributed routing framework of the Coupled Routing and Excess Storage (CREST) model with a new land surface process model that strictly couples water and energy balances at the SVA layer, imposing closed energy balance solutions. The model is vectorized and parallelized to achieve long-term (>30 years) high-resolution (30 m to 500 m and subhourly) simulations of large river basins utilizing high-performance computing. The model is tested in the Connecticut River basin (20,000 km²), where flooding is frequently associated with interactions of snowmelt triggered by rainfall events. Model simulations of distributed evapotranspiration (ET) and snow water equivalence (SWE) at daily time step are shown to match accurately ET estimates from MODIS (average NSCE and bias are 0.77 and 6.79%) and SWE estimates from SNODAS (average correlation and normalized root mean square error are 0.94 and of 19%); the modeled daily river flow simulations exhibit an NSCE of 0.58 against USGS streamflow observations.

© 2017 Elsevier B.V. All rights reserved.

1. Introduction

The water cycle has been extensively studied in terms of land surface modeling (Liang et al., 1994; Ludwig and Mauser, 2000; Wang et al., 2011), yet in mid- and high-latitude regions affected by heavy snow, acceptable performance with a hydrological model is difficult to achieve (Parr et al., 2015). The snow accumulation and melting process in these regions greatly affects both thermal and water budgets (Anderson, 2006, 1976; Bartelt and Lehning, 2002; Lehning et al., 2002a), which in turn control evapotranspiration, soil temperature, and soil moisture calculations. These processes that greatly impact spring flow simulations have been studied extensively by both hydrological and snow process modeling groups. In forested areas, great efforts have been exerted to simulate snow processes (Anderson, 1976; Andreadis et al., 2009; Bartelt and Lehning, 2002; Lehning et al., 2002a; Lehning et al., 2002b; Fu et al., 2014). Even after calibration, however, these model

simulations and observations have agreed only on annual amounts, while the uncertainty in daily values is considerable (Fu et al., 2015). This land surface modeling uncertainty has a great impact on flow simulations (Essery et al., 2009). In addition, most aforementioned snow models are designed merely for one-dimensional simulations, while the distributed hydrological models are suitable for simulations at moderate (>5 km) to macro (>1/8°) scales.

Current hydrological models use concepts from snow models by fully or loosely coupling with their original land surface schemes. For this paper, we applied a strictly closed energy balance (EB) solution to represent snow-affected water cycle processes and interactions with vegetation in forested areas. The difficulty of solving EB lies in structuring the air-vegetation-soil layers under various land surface conditions, formulating thermal/water balance equations within layers and flux/mass exchanges between layers, deriving distributed parameters, and making the nonlinear system within every grid cell converge efficiently. The computations become more challenging when these processes are to be resolved over large regions (ranging from large basins to continents) and long periods (multiple decades) at fine spatiotemporal scales.

^{*} Corresponding author at: Civil and Environmental Engineering, University of Connecticut, Storrs 06250, United States.

E-mail address: xinyi.shen@uconn.edu (X. Shen).

Originating from lumped hydrological models, the linear reservoir routing (LRR) can also be extended to distributed hydrological models with promising efficiency and acceptable accuracy, such as the parallel linear reservoir (PLR) (Lázaro et al., 2015) and fully distributed linear reservoir (FDLRR) (Shen et al., 2016).

Here we describe the development and evaluation of a new model aimed at improving the accuracy of hydrological simulations in snow- and forest-covered regions at fine spatiotemporal resolution (30 m to 500 m and hourly time steps) and for long periods (35 years to 50 years). Specifically, we extended the distributed hydrological framework of the Coupled Routing and Excess STorage (CREST) model (Wang et al., 2011; Shen et al., 2016) to physically integrate hydrological and snow processes, including vegetation interception, evapotranspiration, soil infiltration and snow accumulation, melting, and refreezing. Furthermore, parameters of CREST's runoff generation module are distributed and can be physically derived, while the routing parameters are uniform and can be optimized based on observed stream flow data.

In the next section we describe the development of the model, including its land surface structure and the methodology implemented for coupling water and energy balances. In Section 3 we describe the model validation over the Connecticut River. We discuss the model performance evaluation in Section 4, and in Section 5 we present our conclusions and thoughts on future directions. Abbreviations used in this paper are defined in Table 1.

2. Methodology

2.1. Model overview

We selected the CREST hydrological model as the framework for this study because of its computationally efficient, fully distributed routing module (Shen et al., 2016) that can run large basin ($\sim 10^6$ km²) simulations at fine spatiotemporal resolution (30 m to 1 km spatial grid resolution and hourly time steps) over long periods (a few decades). However, CREST's current simple runoff generation scheme does not explicitly account for vegetation structure or the energy balance—processes that are critical for mid- and high-latitude regions affected by mixed phase precipitation.

In this paper, we extended the CREST model implementing a physically-based runoff generation module that explicitly represents the different vegetation structures and snow processes, as depicted in Fig. 1. The runoff generation module solves for the coupled water and energy balances, using as input dynamic variables—namely, meteorological variables (precipitation, radiation, humidity, wind speed), and leaf area index (LAI)—and static parameters—land cover, soil properties, vegetation species descriptions, and impervious ratios. The new version of CREST is named CREST-SVAS to represent the model's extension in terms of soil-vegetation-atmosphere-snow (SVAS) processes.

Table 1
Abbreviations used in this paper.

Abbreviation	Full Name
CREST	coupled routing and excess storage
SVA	soil-vegetation-atmosphere
SVAS	soil-vegetation-atmosphere-snow
ET	evapotranspiration
SWE	snow water equivalence
EB	energy balance
LAI	leaf area index
NSCE	Nash-Sutcliffe efficiency coefficient
RMSD	root mean squared difference
NRMSD	normalized root mean squared difference
HPC	high performance computer
VIC	variable infiltration capacity

2.2. Characterization of the Soil-vegetation-atmosphere structure

To compute the redistribution of precipitation at the vertical dimension, water and thermal balances must be simultaneously solved. In a given layer, we solve water balance for the water availability, which in turn greatly affects the temperature we solve for in the thermal balance. Knowing the temperature change, we can then estimate the amount of energy that is spent in changing the phase and amount of water.

Accurate modeling of the water and temperature variables depends primarily on the characterization of soil-vegetation-atmosphere (SVA) interactions through coupling of the water and thermal balances. Conceptually, we classify plants into two categories: with canopy and without canopy. The former are able to intercept both snowfall and rainfall, while the latter can only intercept rainfall. Considering the thermal insulator property of snow, temperature differences may occur between the canopy layer, adjacent air and encapsulating air of the canopy layer. The SVA, therefore, is thermally divided into, at most, five layers, as shown in Fig. 1. The snowpack layer vanishes when the ground has no snow accumulation, as does the atmospheric layer when there is no intercepted snow. Snowpack is divided into two layers, the surface layer and pack layer, to mimic the thermal insulator function of a snow layer between soil and air. As in (Liang et al., 1999), soil is thermally divided into two layers and physically divided into three layers. The coupled water and energy balance computational steps based on this conceptual structure are depicted in Fig. 2.

2.3. Water balance

Water exchanges in the rainfall runoff generation module include the interception of precipitation and evapotranspiration (ET) by vegetation; the accumulation and melting of the snow pack, its refreezing, and, finally, the outflow of the pack water; and the percolation by water of multiple soil layers. When precipitation first reaches the SVA structure, it undergoes the interception process if vegetation is present. Then, through-fall triggers the snow accumulation or melting process on the ground if there is snow or if the through-fall itself contains snow. Finally, the outflow from the snowpack or, in a snow-free grid, the through-fall infiltrates soil layers. Meanwhile, ET is taking place, including the evaporation and/or sublimation and/or from intercepted water and transpiration by plants.

2.3.1. Interception by vegetation

Precipitation is partitioned into snowfall and rainfall as a function of surrounding air temperature (Anderson, 2006). Snow interception, then, consists of canopy area accumulation, the blowing of snow from the canopy by wind, and melting-triggered release. Based on previous findings on the dependence of snow interception on vegetation properties and climatic variables (Satterlund and Haupt, 1970), the maximal holding capacity of the canopy is proportional to the LAI (Kobayashi, 1987) and the canopy temperature (Ohta et al., 1993), and the increment of the interception during a time step is proportional to the snowfall (Storck et al., 2002). The snow blowing process is driven by wind speed, following Bowling et al. (2004). Similarly, liquid water interception capacity is affected by the intercepted snow, the LAI, and the temperature, following the method used by (Andreadis et al., 2009).

2.3.2. Snowpack accumulation and ablation

The precipitation remaining after the interception process, together with the released drips from the vegetation layer, form the through-fall precipitation. Solid water contained in the through-fall contributes to the formation of the snowpack on the ground surface, which may contain solid and/or liquid water (if

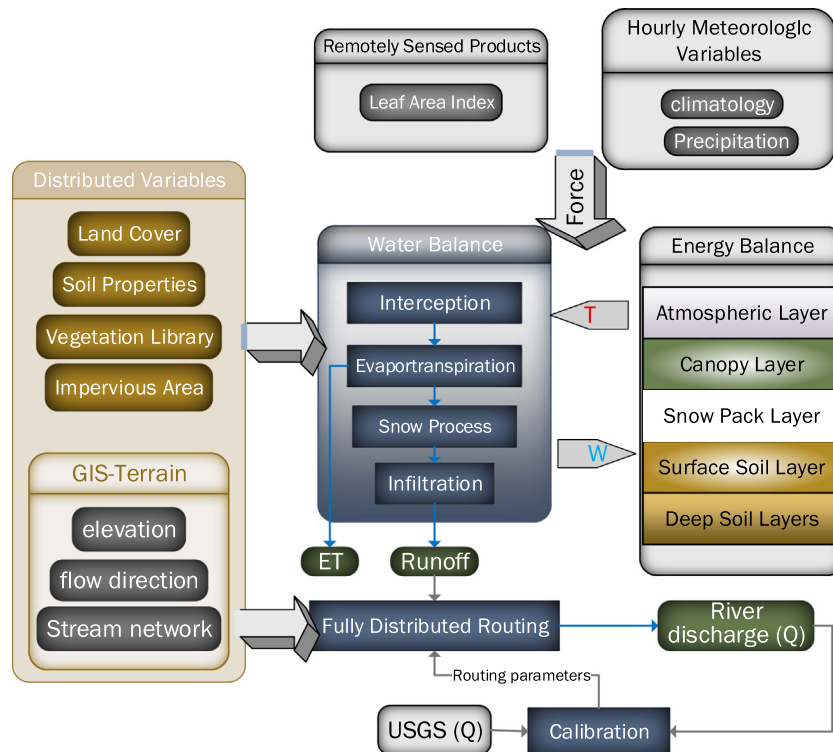


Fig. 1. Interface and structure of the model consisting of a runoff-generation and routing component.

the temperature of the given layer is at 0 °C). Depending on the solid amount, both layers have a certain capacity of liquid water storage that is modeled following Anderson (1976). For simplicity, the SWE boundary between the surface and pack layer is conceptually fixed at 125 mm. In other words, when solid water accumulation on the surface layer does not exceed this fixed SWE amount, no pack layer would exist.

Compaction, in which fresh snow is redistributed into the two-layer structure of the snowpack, is the first step of accumulation. It is followed by the evaporation, sublimation melting, or refreezing process. The amount of evaporation and sublimation is limited by the water availability and determined by the latent heat solved for by the thermal balance computation that is introduced in Section 2.4. Liquid precipitation through-fall first resides in the surface layer and then is drained into the pack layer if the storage reaches the holding capacity of the surface layer. Finally, outflow is generated if the liquid storage exceeds the holding capacity of both layers.

The microphysics of mass and phase change is complicated within the snowpack layer. To model it efficiently without losing overall accuracy, we propose a few rules for accounting for the mass and phase change in the accumulation and ablation process:

- 1) Sublimation only happens after liquid water is evaporated out, and both processes happen only at the surface layer.
- 2) Liquid water in the pack layer does not “go up” unless the capacity of the pack layer is not enough to hold it.
- 3) Melted water is added to the surface layer first. Therefore, ice in the pack is always consumed first during the melting season.

2.3.3. Infiltration

The outflow from snowpack or from through-fall in snow-free areas triggers the infiltration process. CREST uses the variable infiltration curve (Liang and Xie, 2001; Wood et al., 1992; Zhao, 1992;

Zhao and Liu, 1995) to compute the infiltration process in the first moisture layer and the percolation algorithm of the Soil and Water Assessment Tool (SWAT) to account for the vertical moisture transport among soil layers. The variable infiltration curve is widely used in many hydrological models to account for the sub-grid variability of soil heterogeneity. Since the scope of this model development was to improve snowmelt-contributed flood processes, we considered unnecessary the use of a more physical but computationally expensive infiltration method (Richards, 1931; Ross, 1990; Van Dam and Feddes, 2000) at this point.

2.4. Thermal balance

The energy balance (EB) represents the physical consistency but also the modeling complexity of a hydrological model. The complete form of EB in an arbitrary layer of medium can be formulated by Eq. (1),

$$R_n = H + E - G + \Delta H + \Delta M \quad (1)$$

where R_n is the net radiation (W/m^2), H is the sensible heat, E is the latent heat, G is the conductive heat flux, ΔH is the heat storage change of the medium, and ΔM is the heat induced by mass changes. Depending on different land cover and snow conditions, some terms vanish because of insignificance, and neighboring SVA layers (described in Section 2.2) may be combined into one to realize Eq. (1). Sections 2.4.1 through 0 and Fig. 2 describe the new model's realization of equation (1) in different layers and snow conditions.

2.4.1. Thermal balance in the canopy layer

2.4.1.1. Snow-free condition. As shown in Fig. 2(a), when the canopy layer is free of snow, H and ΔH are negligible, and ΔM does not exist. Consequently, the temperature of the canopy can be set to air temperature, and no energy balance needs to be solved. The canopy layer is combined with the layer beneath—namely, the soil

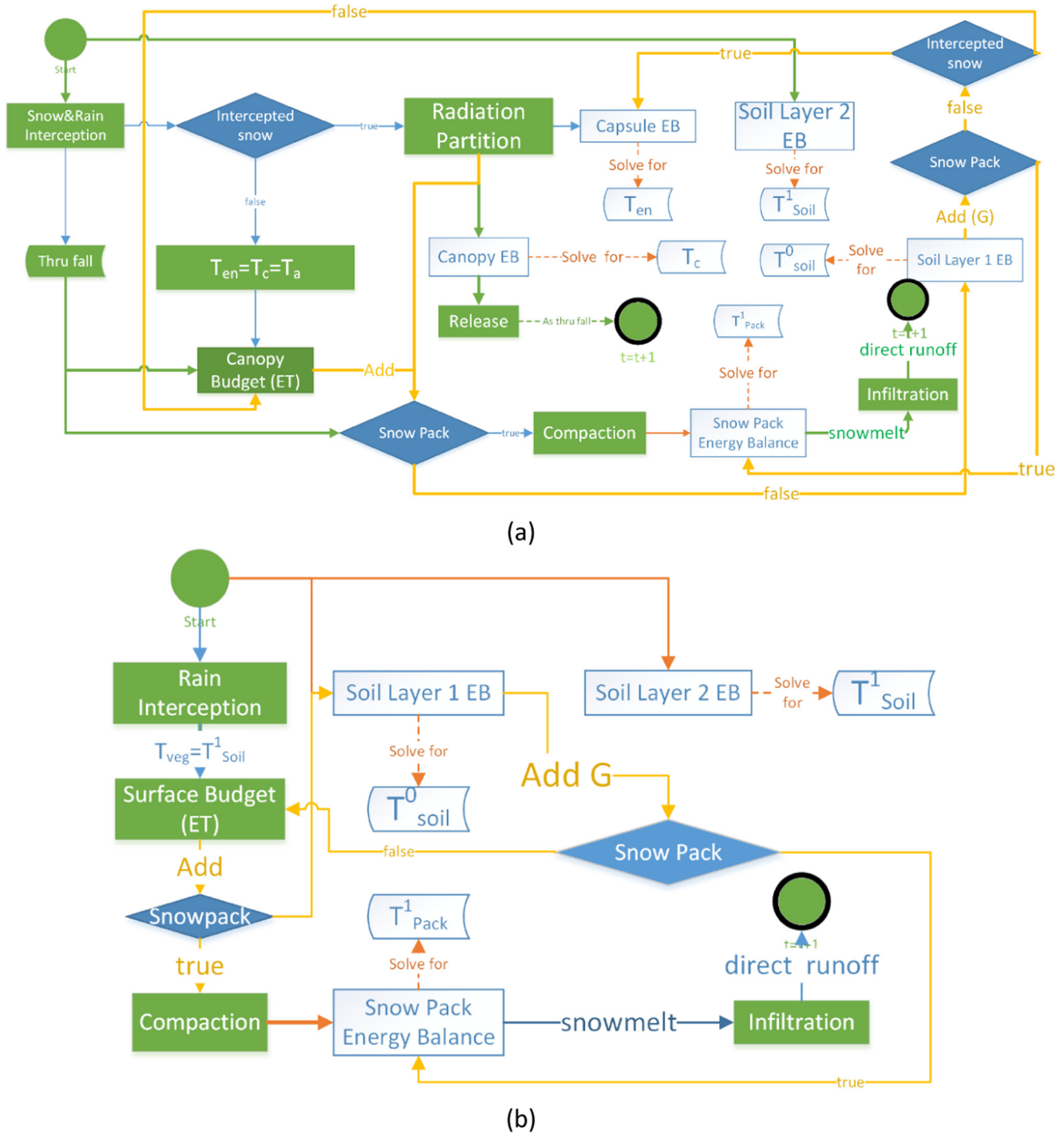


Fig. 2. Coupled Energy Water redistribution module integrated with a snow accumulation and ablation process in condition of (a) the land cover has a canopy layer and (b) the land cover is a short vegetation.

layer or the snowpack layer in the EB equation. The net radiation is given by Eq. (2),

$$R_n = (1 - \alpha_c)R_S + \varepsilon_c[R_L - 2\sigma(T_a + 273.15)^4] \quad (2)$$

where R_S and R_L are downward shortwave and longwave radiation, α_c and ε_c are albedo and attenuation of the canopy layer, $\sigma = 5.67 \times 10^{-8} \text{ W}/(\text{m}^2\text{K}^4)$ is Stefan-Boltzmann constant, and T_a ($^{\circ}\text{C}$) is the air temperature. The first and second terms account for the net shortwave and longwave radiation, respectively. The coeffi-

cient 2 of the outgoing longwave radiation comes from the radiation of the canopy layer to both the hemispheres. The latent heat, E , contributed by the evapotranspiration (ET), can be directly computed by the potential ET (PET), which is given by the Penman-Monteith equation (Allen et al., 1998), and then adjusted by the availability of intercepted liquid water and soil moisture and the moisture resistance of vegetation roots (Liang et al., 1994). The conductive heat, G , represents the ground heat flux is caused by temperature difference between of the solid layers. It vanishes if the understory medium is snowpack—because ice and fresh snow have very little

thermal conductivity—and is given by Eq. (21) if soil is right beneath. Since negligible heat storage can be used to balance Eq. (1), it can be unbalanced, that is,

$$B = R_n + G - E \neq 0 \quad (3)$$

B as the rest term is then cast to the understory layer, which represents the combination mathematically.

2.4.1.2. Snow condition. If snow is intercepted by the canopy layer, the temperature of the intercepted snow, T_{int} ($^{\circ}\text{C}$), is solved for from EB in the canopy layer independently, and the temperature of the encapsulating air of the canopy layer, T_{en} , can be different from T_a and T_{int} . Note that it is valid to employ a one-layer snow model in the canopy layer with uniform temperature, T_{int} , because intercepted snow is always thin. To solve for T_{en} , the EB equation in the encapsulating air layer is formulated as described in Section 0.

As an alternative to Eq. (2), the net radiation of the canopy layer is given by Eq. (4),

$$R_n = \tau(1 + \alpha_s)(1 - \alpha_c)R_s + \varepsilon_c[R_L - 2\sigma(T_{int} + 273.15)^4 + \varepsilon_s\sigma(T_{surf} + 273.15)^4] \quad (4)$$

where c and s represent, respectively, radiation coefficients of the canopy layer and the understory surface. The sensible heat is proportional to the difference between T_{int} and T_{en} ,

$$H = \frac{\rho_a c_p}{r_a}(T_{int} - T_{en}) \quad (5)$$

where ρ_a , c_p , and r_a stand for density of air (kg/m^3), specific heat of air at constant pressure ($\text{J}\cdot\text{kg}^{-1}\text{K}^{-1}$), and wind-adjusted aerodynamic resistance to heat flow (s/m) between the snow surface and the atmosphere at the near-surface reference height, given by (Monteith and Unsworth, 2007).

The latent heat, E , given by Eq. (6), consists of the evaporation of liquid water, E_v , and the sublimation of solid ice, E_s , in the canopy layer upon neglecting transpiration in the snow covering condition,

$$E_{s,v} = L_{s,v}\rho_w \left[\frac{\rho_a}{P_a\rho_w T_a}(e_a - e_{surf}) \right] \quad (6)$$

The second factor (in square brackets) of Eq. (6) stands for the maximal water evaporation rate in depth, which can be limited by the availability of water. In Eq. (6), ρ_a and ρ_w denote the density of air and water (kg/m^3), respectively; P_a is the atmospheric pressure (Pa), and $L_{s,v}$ stand for the specific latent heat of sublimation and evaporation (J/kg) that are computed by Eqs. (7) and (8):

$$L_v = 2.5008 \times 10^6 - 2.36 \times 10^3 T_{int} + 1.6 T_{int}^2 + 0.06 T_{int}^3 \quad (7)$$

$$L_s = 2.8341 \times 10^6 - 293 T_{int} - 4 T_{int}^2 \quad (8)$$

e_a is vapor pressure of the air which is a function of relative humidity and T_{en} , (or specific humidity and P_a); $e_{surf}(T_{int})$ is the vapor pressure (usually assumed saturated) on the surface of the intercepted snow surface. The computation of both can be found in (Allen et al. (1996); Allen et al. (1998)). Note that $E_{s,v}$ is typically negative when sublimation or evaporation occurs, but can be positive if condensation or liquefaction occurs, which indicates the formation of frost or dew, respectively.

ΔM is introduced by the heat deficit contained in intercepted precipitation,

$$\Delta M = \frac{\Delta D_H(T_a, P)}{\Delta t} \quad (9)$$

where P is total precipitation presented as SWE (m).

Heat deficit is defined as the opposite of the minimal energy the snowpack needs to return to isothermal status (0°C):

$$D_H(T, SWE) = c_{ice} \times SWE \times T \quad (10)$$

The heat storage change in intercepted snow comes from two processes, the change of temperature and phase:

$$\Delta H = \frac{D_H(T_{int}, SWE) - D_H(T_{int}^-, SWE)}{\Delta t} + \frac{\rho_w \Delta_{ph} L_f}{\Delta t} \quad (11)$$

where T_{int}^- is the average temperature of intercepted snow during the last time step, SWE_{int} is the total depth of snow water equivalent (m) intercepted by the canopy, while $\Delta_{ph} < 0$ (or $\Delta_{ph} > 0$) is the depth of refrozen (or melted) water, ρ_w is the density of water (kg/m^3), Δt is the duration of the simulation time step (s) and $L_f = 3.337 \times 10^5 \text{J}/\text{kg}$ and $c_{ice} = 2.1 \times 10^6 / \text{m}^3 \cdot ^{\circ}\text{C}^{-1}$ are the latent heat of freezing and specific heat of ice respectively. Physically, all liquid water must be refrozen if $T_{int} < 0$, and all solid water must be melted if $T_{int} > 0$, whereas when $T_{int} = 0$, the amount and direction of the phase change can vary within the limit of availability to balance the energy budget. This variability makes the energy budget as a function of T_{int} non-differentiable and therefore requires modification of the traditional numerical solvers, as described in Section 2.5.

The conductive heat, G , is computed in the same way as when the canopy is snow free.

2.4.2. Thermal balance in the snowpack

The physics of the EB in the snowpack layer is similar to that of the EB in intercepted snow. The difference originates from the two-layer structure of the snowpack and the heat exchange between the snowpack and the soil. The thermal insulator property of snow is utilized by setting thermal conductivity to zero in both the surface and pack layer. In other words, heat cannot be conducted either upward or downward via a layer of snow until the layer has been entirely melted. Therefore, it is valid to assume that both the surface and pack layer of snow are of uniform temperature— T_{pack}^1 and T_{pack}^2 , respectively. Consequently, a concise way of accounting for the heat exchange in the two-layer structure is through the delegation of D_H . Compaction redistributes heat deficit in the two layers proportionally to the amount of mass it redistributes as following:

$$\Delta M_H^j = \frac{\Delta SWE^{i-j}}{SWE^i} D_H^i - \frac{\Delta SWE^{j-i}}{SWE^j} D_H^j + \frac{\Delta thru^j}{thru} D_H^{thru} \quad (12)$$

where superscript i and j stand for the surface and pack layer of the snow pack, respectively, and $thru$ refers to the through-fall. Once the heat deficit of a snow layer is changed due to compaction, the new temperature is immediately obtained from Eq. (10).

In the EB of the surface snow layer, H , E , and ΔH can be computed using Eqs. (5), (6), and (11) by substituting T_{pack}^1 for T_{int} . The conductive heat, G , only exists when the pack layer vanishes and is computed by Eq. (21). The net radiation is given by

$$R_n = (1 - \alpha_s)(1 - \tau)(1 - \alpha_c)R_s + \varepsilon_s \sigma \left[\varepsilon_c (T_c + 273.15)^4 - (T_{pack}^1 + 273.15)^4 \right] \quad (13)$$

where T_c is T_a if the canopy is snow-free, or T_{int} otherwise.

In the EB of the pack layer, R_n , E , and H vanish for the pack layer, and ΔH is computed in the same way as in the surface layer, using T_{pack}^2 instead of T_{pack}^1 . G is computed by Eq. (21).

2.4.3. Thermal balance in soil layers

To solve the EB in the soil layers, a temperature profile is assumed. We adopted the two-layer thermal and three-layer moisture soil profile structure as described in (Liang et al., 1999), where temperature changes linearly with depth in the first thermal layer and exponentially below it, as in (14) and (15):

$$T(z) = T_{soil}^0 + \frac{z}{d_1}(T_{soil}^1 - T_{soil}^0), \quad 0 < z < d_1 \quad (14)$$

$$T(z) = T_{soil}^2 + e^{-\frac{z-d_1}{d_p}}(T_{soil}^1 - T_{soil}^2), \quad z \geq d_1 \quad (15)$$

where d_1 , d_2 , and d_p represent the thickness of the first and second thermal layers and the dampen depth, respectively.

The conductive heat flux within soil layers is given by Eq. (16),

$$G = -\kappa \frac{\partial T}{\partial z} \quad (16)$$

where κ is the thermal conductivity of the soil (in $Wm^{-1}K^{-1}$) and z is depth (in m).

Since conductive heat exchange exists only between soil layers, the temperature of the boundary between the first and second layers, T_{soil}^1 , can be solved for using the EB in the second thermal layer, as given by Eq. (17),

$$T_{soil}^1 = \frac{A \times T_{soil}^{1-} + B \times T_{soil}^0 + C \times T_{soil}^2}{A + B + C} \quad (17)$$

where T_{soil}^{1-} is the boundary temperature between the first and second soil layer during the last time step and T_{soil}^2 is the dampen temperature in the very deep soil, which does not change significantly with time; parameters A , B and C are defined below:

$$A = c_{p-soil}^2 \times d_p(1 - e^{-d_2/d_p})/\Delta t \quad (18)$$

$$B = \kappa^1/2d_1 \quad (19)$$

$$C = -\kappa^2(0.5 - e^{-d_2/d_p})/d_p \quad (20)$$

where c_{p-soil}^i and κ^i are the specific heat and thermal conductivity of the i th soil layer. Therefore, T_{soil}^0 is the only unknown we need to solve for numerically, using the EB of the surface soil layer.

Substituting Eq. (14) for (16), the conductive heat (ground flux, $G \uparrow$) from the surface soil layer to the upper space is given by

$$G \uparrow = -\kappa \left(\frac{T_{soil}^1 - T_{soil}^0}{d_1} \right) \quad (21)$$

The total conductive heat loss in the first layer is given by:

$$G = 0.5 \left[G \uparrow - \frac{\kappa^2}{d_p} (T_{soil}^2 - T_{soil}^1) \right] \quad (22)$$

The net radiation, R_n , and sensible heat, H , recede to zero when snowpack is present. Otherwise, R_n is computed by Eq. (13), and H is calculated by Eq. (5), replacing T_{int} with T_{soil}^0 and recalculating the r_a value at the height of soil roughness. In case a vegetation cover exists, the energy consumed by ET has been accounted for in the canopy layer. Then the latent heat, E , in soil layers vanishes to zero.

In the bare soil case, soil water can be evaporated in two different ways: either from the first moisture layer at rate R_E , given by the Arno model (Franchini and Pacciani, 1991), and the consumed energy is calculated by the following equation:

$$E = L_s \rho_w R_E \quad (23)$$

or from three layers at different resistance, as in (Wang et al., 2011). We have created user options for these two different evaporation algorithms for bare soil.

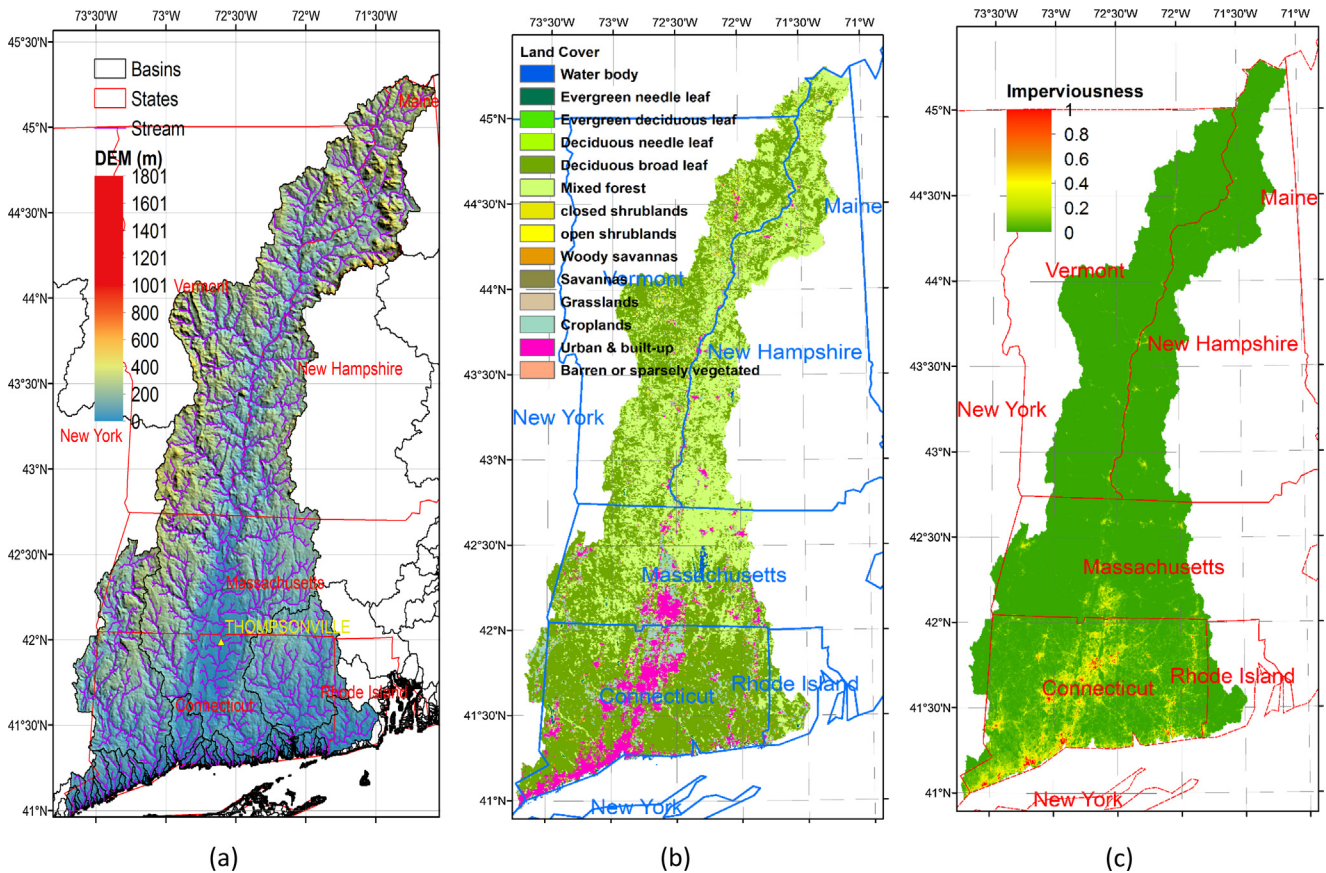


Fig. 3. Description of the testing basin region including (a) terrain, (b) land cover type and (c) imperviousness.

2.4.4. Thermal balance in the encapsulating atmosphere

As discussed in Section 2.4.1, the EB equation for the surrounding air needs to be solved when snow is intercepted. R_n , E , ΔM , and ΔH vanish in this air layer. The sensible heat in this layer is the sum of the sensible heat of the canopy, the understory, and the above air. If the ground is free of snow, G needs to be added to the EB of this layer.

2.5. Numerical solver of the EB equation-set

Each white block in Fig. 2 represents an EB equation to solve. Since sensible and conductive heat may be exchanged across layers, however, the temperature of neighboring layers affects the EB of the given layers. Therefore, solving EB is equivalent to solving a set of nonlinear equations.

As mentioned in Section 2.4.2, the non-differentiable EB as a function of the snow temperature cannot be solved by traditional numerical solvers. Consequently, we implemented the modified Broyden's method (Press, 2007). When snow exists only on the ground, T_{pack}^1 and T_{soil}^0 are the two unknown temperatures to solve for. We first set T_{pack}^1 to zero and solve for T_{soil}^0 . If the convergence is achieved within a limited number of iterations, the solution is found and the solver exits. Otherwise, it indicates that T_{pack}^1 is not zero, and then we treat both T_{pack}^1 and T_{soil}^0 as unknowns and solve the equation-set again. Naturally, if snow exists both on the canopy and the ground, the EB system will be solved with up to four iterations. This modification successfully resolves the convergence problem and reduces the number of iterations. In practice, we set ten as the maximal iteration times for one trial. It usually takes

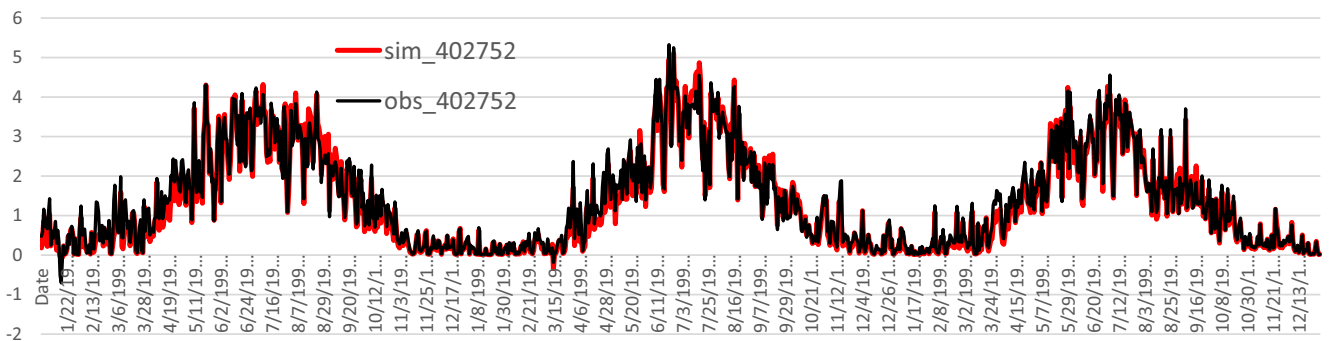
four to five iterations to converge. Consequently, closed energy balance is always achieved in the simulation of a land surface process.

Applying the numerical solver at fine spatiotemporal resolution is computationally expensive. For this reason, we implemented the model on a high-performance computer (HPC) and used ~200 cores for simulating the land surface process. Parallel computation was implemented by evenly distributing basin grids to different cores. Moreover, within each core, vectorization was applied to optimize the computational efficiency of the equation solvers (Van Der Walt et al., 2011). Vectorization was implemented using the MATLAB platform, which further increased the computational efficiency (by around one to two orders) by avoiding looping over grids. Maximum efficiency can be achieved if each core has an independent cache.

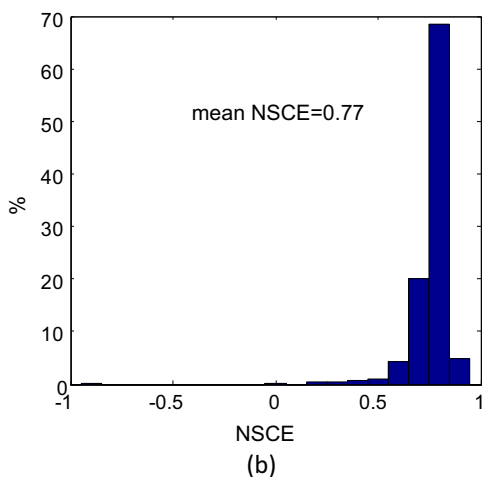
2.6. Routing by modified FDLRR

The Fully Distributed Linear Reservoir Routing (FDLRR) method (Shen et al., 2016, 2014) developed for CREST has been demonstrated to accurately model channel flows. As the kernel of CREST v2.1, however, the FDLRR has not been tested over high-latitude basins affected by heavy snowfall.

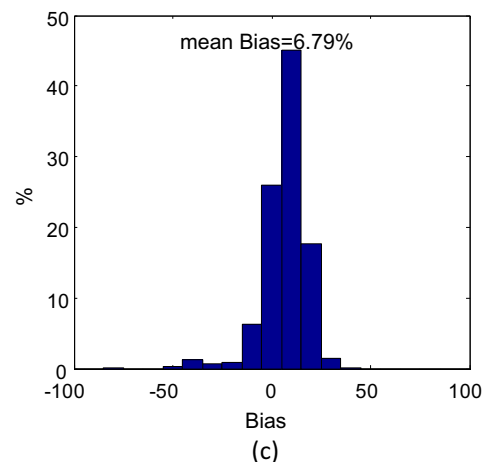
Although the delay of the basin response to precipitation caused by snow accumulation and ablation has been addressed by the precipitation runoff module, it is difficult to physically model the consumed time by (1) the vertical drainage of liquid water in snowpack and (2) the refreezing of overland flow. Available methods (Anderson, 2006) significantly underestimate this delay by neglecting (2), thus resulting in underestimation of flow peak during snowmelt-contributing events. To address this issue empiri-



(a)



(b)



(c)

Fig. 4. Validation of the Actual ET. a) CREST simulation vs. MODIS retrieved ET product in daily scale over a randomly selected 8 km × 8 km grids. b)-c) gives the distribution of error metrics between the simulation and observation over all grids including: c) the NSCE value, d) the relative bias in (%).

cally, we added a time lag parameter (in time step) of snowmelt flow that can be optimized through calibration.

2.7. Error metrics

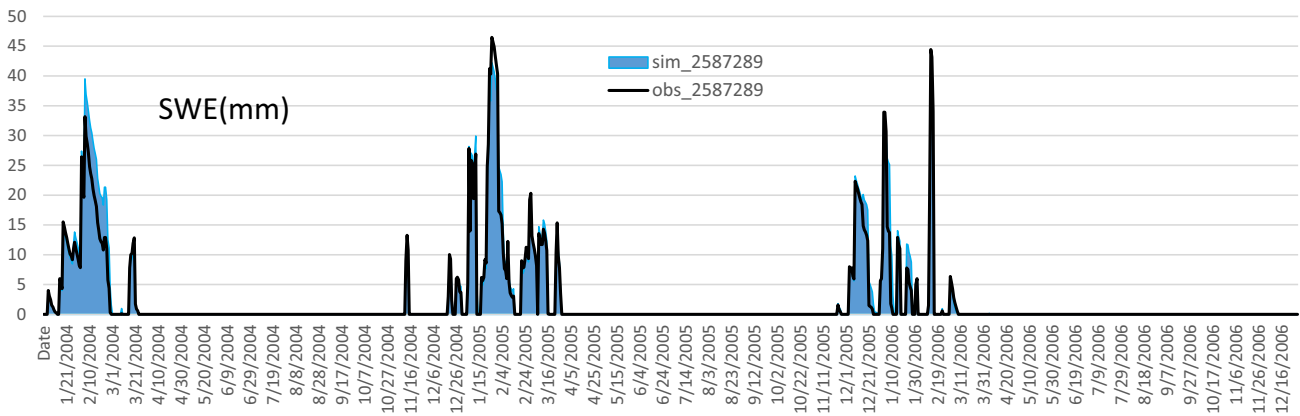
Pearson correlation (R), root mean squared difference (RMSD), and normalized RMSD (NRMSD), given by equations (24) and (25), are used as error metrics of SWE. The concentration at high R value (0.9–1) and low NRMSD (0.1–0.7), shown in Fig. 5(c)–(e), suggests good performance on simulating SWE. The Nash-Sutcliffe coefficient (NSCE), given by equation (26), and relative bias are employed to assess the ET simulation. Concentration at high NSCE (0.7–0.9) and low relative bias (–5% to 10%) indicates good performance on simulating ET.

$$R = \frac{\sqrt{\sum (Q_{sim} - \bar{Q}_{sim})(Q_{obs} - \bar{Q}_{obs})}}{\sqrt{\sum (Q_{sim} - \bar{Q}_{sim})^2} \sqrt{\sum (Q_{obs} - \bar{Q}_{obs})^2}} \tag{24}$$

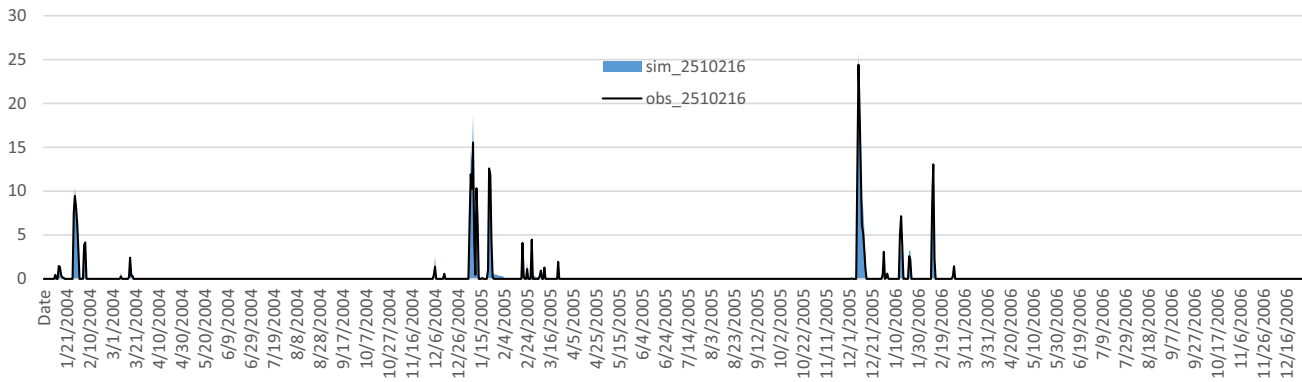
$$NRMSD = \frac{RMSD}{mean} = \frac{\sqrt{N \sum (Q_{sim} - Q_{obs})^2}}{\sum Q_{obs}} \tag{25}$$

$$NSCE = 1 - \frac{\sum (Q_{sim} - Q_{obs})^2}{\sum (Q_{obs} - \bar{Q}_{obs})^2} \tag{26}$$

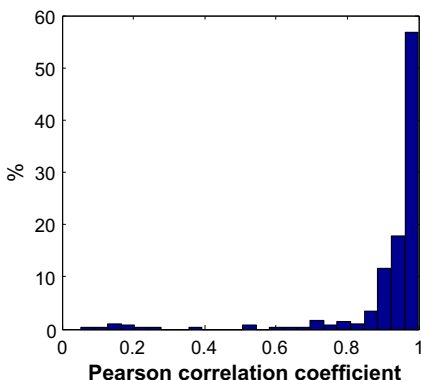
where Q_{sim} and Q_{obs} stand for the time series of interest given by simulation and observation, \bar{Q} represents the mean value of the variable, and N is the number of the time steps.



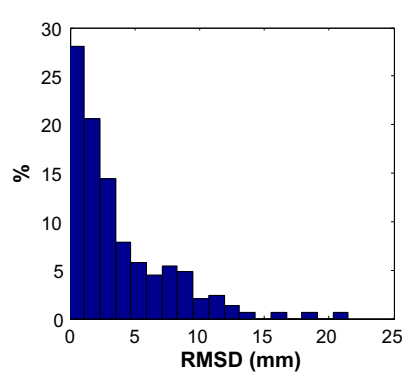
(a)



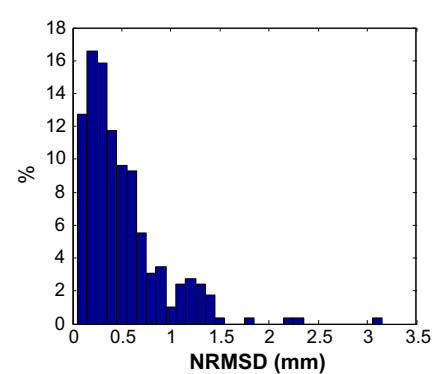
(b)



(c)



(d)



(e)

Fig. 5. Validation of SWE of the ground snowpack. a) and b) give CREST simulation vs. SNODAS “observation” in daily scale over two randomly selected 8 km × 8 km grids including a) a grid experienced heavy snow accumulation and b) a grid experienced light snow accumulation. c)–e) give the distribution of error metrics between the simulation and observation over all grids including: c) the Pearson correlation value, d) the root mean squared difference (RMSD) in millimeter and e) the normalized root mean squared difference, RMSD normalized by mean value.

3. Data, study area, and model parameterization

3.1. Input datasets and model parameters

Various meteorological and remote-sensing forcing data, and static model parameters, including vegetation, soil hydraulic, and land use parameters, are needed to run the precipitation-runoff module of CREST-SVAS. The datasets used in this study are listed in Table 2. The North American Land Data Assimilation System (NLDAS-2) meteorological dataset (Xia et al., 2012a,b) and the GLASS Leaf Area Index (LAI) have records of more than 30 years and were selected for this study to represent our forcing data. Land cover was obtained from the Moderate-Resolution Imaging Spectroradiometer (MODIS) land cover product, MOD12Q1, which defines the 500-meter grid resolution of the simulation. The impervious ratios were extracted from the Connecticut's Changing Landscape (CCL) and the National Land Cover Databases (NLCD) at 30 m resolution that are classified based on the Landsat surface reflectance, and then aggregated to the 500 m model-grid resolution. The vegetation parameter table (listed in Table 3) defines the vegetation properties that affect the ET rate and thermal aerodynamics and was obtained from (Calder and Maidment (1992), Ducoudré et al. (1993), Jackson et al. (1996)). Soil hydraulic properties were computed based on Saxton and Rawls (2006), using the 0–2 m (six-layered) soil characteristics from SoilGrids (Hengl et al., 2014). The study period supported by the atmospheric and LAI datasets is 1979–2012. Simulations were performed at hourly time step.

The routing module of CREST requires terrain data, including the digital elevation model (DEM), flow direction (FDR), and stream network. Global maps of these datasets at 3, 15, and 30 arc-secs can be obtained from maps based on Shuttle Elevation Derivatives at multiple Scales (HydroSHEDS) (Lehner et al., 2006). The U.S. maps can be obtained from the National Hydrographic Dataset (NHD) (Simley and Carswell, 2009) at 30 m spatial resolution. In this study, we used the 15 s (~500 m) version of the HydroSHEDS

Table 2
Distributed Parameters used in the CREST v3.0.

	Variable	Source	Spatial Resolution	Temporal Resolution
Dynamic Weather Forcing	total precipitation air temperature downward shortwave radiation downward long wave radiation humidity (specific or relative) pressure wind speed	NLDAS2 (http://ldas.gsfc.nasa.gov/nldas/NLDAS2forcing.php)	0.125°	1 h
Dynamic Surface Property	LAI	GLASS LAI (http://www.glcfc.umd.edu/data/lai/)	0.05° (~5.5 km) (1982–1999) 1 km (2000–present)	8 days
Static Parameters	Vegetation Parameters Table	(Calder and Maidment (1992), Ducoudré et al. (1993), Jackson et al. (1996))	N/A	monthly periodic
	Land Cover	MCD12Q1 (https://lpdaac.usgs.gov/dataset_discovery/modis/modis_products_table/mcd12q1)	500 m	1 year
	Impervious Area Fraction	Connecticut's Changing Landscape (http://clear.uconn.edu/Projects/landscape/index.htm) National Land Cover Database (http://www.mrlc.gov/nlcd2011.php)	30 m	1 year
	Saturated hydraulic conductivity Field Capacity Wilting point soil moisture Saturated Soil Moisture Organic matter Bulk density	Soil hydraulic properties are computed by the Saxton's model (Saxton and Rawls, 2006) using soil texture and characteristics downloaded from SoilGrids (https://soilgrids.org)	1 km/250 m	N/A
	Routing Parameters	Calibration. Definition please See (Shen et al., 2016; Wang et al., 2011)	Uniform	N/A

Table 3

Vegetation parameters. All parameters are cover-type dependent and parameters before h_{wind} changes every month.

Parameter	Description	Unit
α	Shortwave albedo	N/A
r	Roughness length	m
h	Displacement height	N/A
h_{wind}	Wind measured height	m
tr_0	Minimum incoming shortwave radiation to trigger transpiration	W/m ²
τ_R	Radiation attenuation factor	N/A
τ_{wind}	Wind speed attenuation factor	N/A
b_c	Whether the type Has a canopy layer	true/false
r_{trunk}	Trunk ratio	N/A
$d_i, i = 1,2,3$	Root zone thickness	m
$f_i, i = 1,2,3$	Root zone fraction	N/A
r_0	minimum stomatal resistance to evaporation	s/m
r_c	Architectural resistance to evaporation	s/m

dataset. Routing parameters, except the newly developed snowmelt-runoff time lag (discussed in Section 2.6), are inherited from the previous version of CREST (Shen et al., 2016). Since routing parameters are either conceptual or difficult to derive on a physical basis, we optimized them using the automated Shuffled Complex Evolution University of Arizona (SCEUA) algorithm (Duan et al., 1993, 1992).

3.2. Study area

We tested our modeling framework based on the Connecticut River Basin, a complex terrain that represents a drainage area of ~29,200 km² and the maximal, minimal and mean elevation of 1801 m, 0 m, and 303.97 m respectively, as shown in Fig. 3(a). The Connecticut River originates at the U.S. border between Quebec and New Hampshire; it then drains via Vermont, New Hampshire, Massachusetts, and Connecticut and discharges into the Long Island Sound. Snowmelt in the study basins significantly con-

tributes to spring flows and flood events, while rainfall from storms primarily contributes to the floods occurring in summer and autumn. The climate type of the study region is humid conti-

ental. Over the basin, the average annual snowfall and rainfall are 164 mm and 1064 mm in equivalent water depth while rainfall spreads throughout the year. Therefore, solid, liquid, and mixed

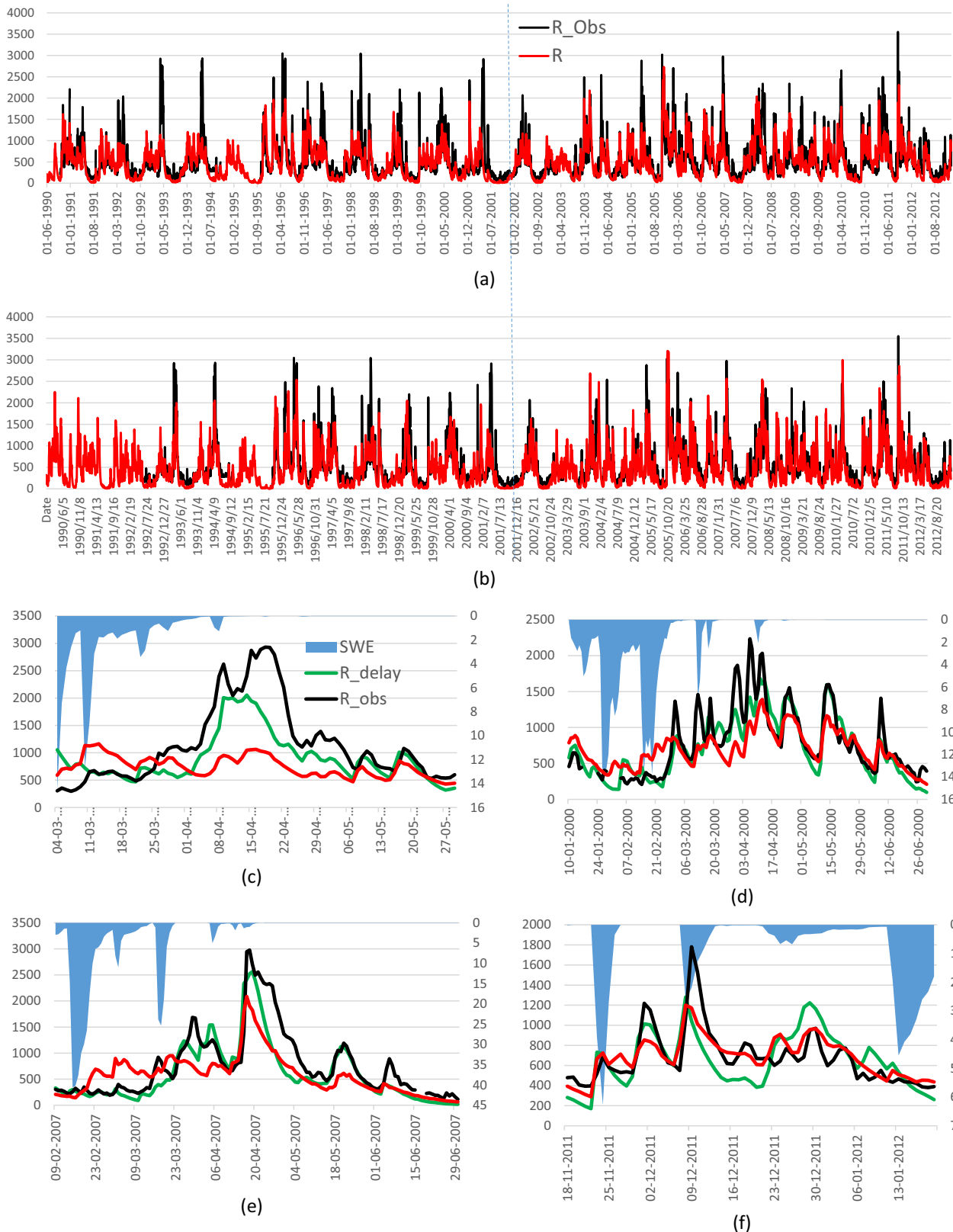


Fig. 6. Daily flow validation against observation including simulation (a) without and (b) with considering the time lag of snowmelt caused flow. (c) to (f) show four spring flood events contributed by snowmelt in 1994, 2000, 2007 and 2012.

precipitation are all experienced over the study area. Deciduous broadleaf and mixed forest dominate the overland area, buildings take up a large fraction along the downstream of the Connecticut River and coast, and agricultural lands are distributed along the Connecticut River, as suggested by Fig. 3(b). As the imperviousness in a given area depends on how built up the area is, it is high along the downstream of the Connecticut River and coast, as shown by Fig. 3(c). The densely distributed vegetation and canopy cover, as well as the meteorological conditions of the region, indicate a need to explicitly account for snow interception, accumulation and ablation, as well as evapotranspiration processes over the basin.

4. Results and model validation

Both the simulated land surface variables and stream flows were used in this study to evaluate the accuracy of the proposed model. Specifically, we used ET and SWE of the snowpack datasets (Section 4.1) retrieved from satellite observations and through data assimilation, respectively, and U.S. Geological Survey stream flow measurements in the Connecticut River (Section 4.2).

4.1. Validation of land surface simulations

The simulated ET and the snowpack in SWE were validated against third-party observations. The simulated ET was compared against the MODIS ET product (Zhang et al., 2010) and the simulated SWE of the snowpack against the SWE in the Snow Data Assimilation System (SNODAS) dataset (<https://nsidc.org/data/g02158>). Both are regarded as the best available gridded reference datasets for validation of the model ET and SWE parameters (Tedesco and Narvekar, 2010). To moderate random error effects, variables of the land surface process are conventionally validated at basin-average (or one-gauge point) and monthly time scale (Liang et al., 1994; Parr et al., 2015). With such averaging, however, one cannot evaluate the modeling skill at fine spatiotemporal resolution, which is critical to many applications, such as simulation of flood processes. In this study, we strictly validated our model's simulated ET and SWE parameters at high spatial resolution, namely 8 km × 8 km grid cells, which represents the spatial resolution of MODIS ET, and at daily temporal resolution. Since the model ran at 500 m spatial resolution and hourly time step, model outputs were averaged spatially within each 8 km × 8 km grid cell and aggregated to daily. The SWE outputs of the ground snowpack were also averaged within the same spatiotemporal scale.

The validation results of ET and SWE variables are given in Fig. 5 and Fig. 4, respectively. The average NSCE and average relative bias of simulated ET vs. the MODIS daily ET product are 0.77 and 6.79%. The average correlation of and normalized root mean square error of SWE estimates of simulation vs. SNODAS are 0.94 and 19%.

Using the HPC computational resources as introduced in Section 2.5, we were able to complete the computation over 180,000 grid cells and 298,008 time steps (~34 years at hourly time step) within 40.6 h. This performance is the combined effect of using parallel and vectorized computation.

4.2. Validation of the stream flow simulations

Fig. 6 compares the CREST stream flow simulations against the USGS observations at Thompsonville (gauge No. 01184000, denoted by the green triangle in Fig. 3) during 1990–2012, the period for which the USGS flow data are available. The model simulation with the snowmelt time-lag being optimized as 26 days (Fig. 6(b)) exhibits better agreement with USGS stream flows than the simulation without the lag parameter (Fig. 6(a)). The NSCE of the entire period increases from 0.42 to 0.58, while the NSCE of the

timespan after 2002 increases from 0.60 to 0.63. The necessity of the snowmelt time lag adjustment parameter is consolidated by examining spring floods, shown in Fig. 6(c) and (f), when the snowpack is considerably melted. The simulation without the time lag adjustment (red line) tends to overestimate significantly the flow rate before the real floods are formed. As a consequence, during the actual peak time, the simulation underestimates the actual peak flow.

The time lag effectively addresses this problem, capturing the flood peaks during snowmelt periods (green line) without affecting the flood hydrographs during the summer and fall flood periods. The evidently low model performance shown in Fig. 6(a) from 1990 to 2001 is because the major floods during the first decade were mostly spring floods, whose peak values were significantly underestimated without delaying snowmelt-contributed flow. In the second decade (2002–12), due to possible global warming effects (warmer winters), autumn floods became dominant in most years, in which the model performance was not affected by the time lag. Fig. 6(c)–(f) not only verify that snowmelt-contributed flood events are well captured by the proposed model; they also demonstrate the value of introducing the snowmelt flow delay factor.

Due to the significant contribution of snowmelt, floods in the Connecticut River Basin have not been well captured by existing models (Dis et al., 2015; Parr et al., 2015). Most of these applications have reported NSCE scores of daily discharge simulations around 0.3. As shown in this section, the model proposed in this study improves simulation accuracy by physically coupling the snow accumulation/ablation with other water cycle processes in the SVA structure.

5. Closing remarks

In this paper, we presented the development of a high-resolution hydrological modeling framework aimed at improving simulations of snow-affected runoff generation processes, which are commonly expected in mid- and high-latitude regions. The model is physically based and integrates the most advanced energy balance concepts with remote sensing, atmospheric, soil survey, and GIS datasets. A new snowmelt flow delay parameter was introduced to better capture the magnitude and timing of snowmelt contributions to flood events. Without calibration, the precipitation-runoff module predicted ET and SWE variables with higher accuracy than what has been reported in past studies. This improved representation of snow processes in runoff generation improved the accuracy of stream flow simulations relative to performances reported in previous studies for this region.

Due to its computational efficiency and strong physical basis, this model can be used to conduct long term (>30 years) and high-resolution hydrological simulations at regional scale and for complex snow-affected basins. The accuracy reported in this study indicates that the model can be effectively applied to support physically-based estimations of flood frequencies of ungauged basins, by capitalizing on available long-term atmospheric reanalysis datasets that can span longer periods (35–50 years) than available hourly USGS flow datasets. Furthermore, the adaption of high resolution has prepared the model for future high-resolution meteorological data forcing in a comparable resolution (Zhang et al., 2016).

Acknowledgments

The current study was jointly supported by a research Grant from the Connecticut Department of Energy and Environmental Protection and Natural Science Foundation of China (NSFC), Gen-

eral Program, No. 41471430 and a research Grant from Eversource Energy. The authors would like to thank authors and developers of the datasets used in this study. These are HydroSHEDS by World Wildlife fund Inc. (WWF), NLDAS2 by NASA Land Data Assimilation System (LDAS), SoilGrid by International Soil Reference and Information Centre (ISRIC), NLCD by USGS, CCL by Center for Land Use Education and Research (CLEAR), UCONN, stream flow observations by USGS, LAI product by University of Maryland and MOD12Q1 by Land Processes Distributed Active Archive Center (LP DAAC) NASA.

References

- Allen, R. et al., 1996. Chapter 4 Evaporation and Transpiration in ASCE Handbook of Hydrology. New York, NY, pp. 125–252.
- Allen, R.G., Pereira, L.S., Raes, D., Smith, M., 1998. Determination of ET_0 . Crop Evapotranspiration-Guidelines for Computing Crop Water Requirements-FAO Irrigation and Drainage Paper 56. FAO, Rome, p. 309.
- Anderson, E., 2006. Snow accumulation and ablation model-SNOW-17. On-line documentation.
- Anderson, E.A., 1976. A point of energy and mass balance model of snow cover. NOAA Tech. Rep. NWS 19, 1–150.
- Andreadis, K.M., Storck, P., Lettenmaier, D.P., 2009. Modeling snow accumulation and ablation processes in forested environments. *Water Resour. Res.* 45 (5).
- Bartelt, P., Lehning, M., 2002. A physical SNOWPACK model for the Swiss avalanche warning: Part I: numerical model. *Cold Reg. Sci. Technol.* 35 (3), 123–145.
- Bowling, L., Pomeroy, J., Lettenmaier, D., 2004. Parameterization of blowing-snow sublimation in a macroscale hydrology model. *J. Hydrometeorol.* 5 (5), 745–762.
- Calder, I.R., Maidment, D., 1992. *Hydrologic Effects of Land-use Change*. McGraw-Hill Inc.
- Dis, M., Anagnostou, E., Zac, F., Vergara, H., Hong, Y., 2015. Evaluating multi-scale flow predictions for the Connecticut River Basin. *Hydrol.: Curr. Res.* 6 (2), 1.
- Duan, Q., Gupta, V.K., Sorooshian, S., 1993. Shuffled complex evolution approach for effective and efficient global minimization. *J. Optim. Theory Appl.* 76 (3), 501–521.
- Duan, Q., Sorooshian, S., Gupta, V., 1992. Effective and efficient global optimization for conceptual rainfall-runoff models. *Water Resour. Res.* 28 (4), 1015–1031.
- Ducoudré, N.I., Laval, K., Perrier, A., 1993. SECHIBA, a new set of parameterizations of the hydrologic exchanges at the land-atmosphere interface within the LMD atmospheric general circulation model. *J. Clim.* 6 (2), 248–273.
- Essery, R. et al., 2009. SNOWMIP2: an evaluation of forest snow process simulations. *Bull. Am. Meteorol. Soc.* 90 (8), 1120–1135.
- Franchini, M., Pacciani, M., 1991. Comparative analysis of several conceptual rainfall-runoff models. *J. Hydrol.* 122 (1–4), 161–219.
- Fu, C., James, A.L., Yao, H., 2014. SWAT-CS: Revision and testing of SWAT for canadian shield catchments. *J. Hydrol.* 511, 719–735.
- Fu, C., James, A.L., Yao, H., 2015. Investigations of uncertainty in SWAT hydrologic simulations: a case study of a canadian shield catchment. *Hydrol. Processes* 29 (18), 4000–4017.
- Hengl, T. et al., 2014. SoilGrids1km—global soil information based on automated mapping. *PLoS One* 9 (8), e105992.
- Jackson, R. et al., 1996. A global analysis of root distributions for terrestrial biomes. *Oecologia* 108 (3), 389–411.
- Kobayashi, D., 1987. Snow accumulation on a narrow board. *Cold Reg. Sci. Technol.* 13 (3), 239–245.
- Lázaro, J.M., Navarro, J.Á.S., Gil, A.G., Romero, V.E., 2015. A new adaptation of linear reservoir models in parallel sets to assess actual hydrological events. *J. Hydrol.* 524, 507–521.
- Lehner, B., Verdin, K., Jarvis, A., 2006. *HydroSHEDS technical documentation, version 1.0*. World Wildlife Fund US, Washington, DC: pp. 1–27.
- Lehning, M., Bartelt, P., Brown, B., Fierz, C., 2002a. A physical SNOWPACK model for the Swiss avalanche warning: Part III: meteorological forcing, thin layer formation and evaluation. *Cold Reg. Sci. Technol.* 35 (3), 169–184.
- Lehning, M., Bartelt, P., Brown, B., Fierz, C., Satyawali, P., 2002b. A physical SNOWPACK model for the Swiss avalanche warning: Part II. Snow microstructure. *Cold Reg. Sci. Technol.* 35 (3), 147–167.
- Liang, X., Lettenmaier, D.P., Wood, E.F., Burges, S.J., 1994. A simple hydrologically based model of land surface water and energy fluxes for general circulation models. *J. Geophys. Res. Atmos.* 99 (D7), 14415–14428.
- Liang, X., Wood, E.F., Lettenmaier, D.P., 1999. Modeling ground heat flux in land surface parameterization schemes. *J. Geophys. Res. Atmos.* 104 (D8), 9581–9600.
- Liang, X., Xie, Z., 2001. A new surface runoff parameterization with subgrid-scale soil heterogeneity for land surface models. *Adv. Water Resour.* 24 (9), 1173–1193.
- Ludwig, R., Mauser, W., 2000. Modelling catchment hydrology within a GIS based SVAT-model framework. *Hydrol. Earth Syst. Sci. Discuss.* 4 (2), 239–249.
- Monteith, J., Unsworth, M., 2007. *Principles of Environmental Physics*. Academic Press.
- Ohta, T., Hashimoto, T., Ishibashi, H., 1993. Energy budget comparison of snowmelt rates in a deciduous forest and an open site. *Ann. Glaciol.* 18, 53–59.
- Parr, D., Wang, G., Bjerklie, D., 2015. Integrating remote sensing data on evapotranspiration and leaf area index with hydrological modeling: impacts on model performance and future predictions. *J. Hydrometeorol.* 16 (5), 2086–2100.
- Press, W.H., 2007. *Numerical recipes 3rd edition: The art of scientific computing*. Cambridge University Press.
- Richards, L.A., 1931. Capillary conduction of liquids through porous mediums. *J. Appl. Phys.* 1 (5), 318–333.
- Ross, P., 1990. Efficient numerical methods for infiltration using Richards' equation. *Water Resour. Res.* 26 (2), 279–290.
- Satterlund, D.R., Haupt, H.F., 1970. The disposition of snow caught by conifer crowns. *Water Resour. Res.* 6 (2), 649–652.
- Saxton, K., Rawls, W., 2006. Soil water characteristic estimates by texture and organic matter for hydrologic solutions. *Soil Sci. Soc. Am. J.* 70 (5), 1569–1578.
- Shen, X., Hong, Y., Zhang, K., Hao, Z., 2016. Refining a Distributed Linear Reservoir Routing Method to Improve Performance of the CREST Model. *Journal of hydrologic Engineering*: 04016061.
- Shen, X., Hong, Y., Zhang, K., Hao, Z., Wang, D., 2014. CREST v2. 1 Refining by a Distributed Linear Reservoir Routing Scheme. AGU Fall Meeting Abstracts, pp. 0918.
- Simley, J.D., Carswell Jr, W.J., 2009. The national map—hydrography.
- Storck, P., Lettenmaier, D.P., Bolton, S.M., 2002. Measurement of snow interception and canopy effects on snow accumulation and melt in a mountainous maritime climate, Oregon, United States. *Water Resour. Res.* 38 (11).
- Tedesco, M., Narvekar, P.S., 2010. Assessment of the NASA AMSR-E SWE Product. *IEEE J. Sel. Topics Appl. Earth Obs.* 3 (1), 141–159.
- Van Dam, J.C., Feddes, R.A., 2000. Numerical simulation of infiltration, evaporation and shallow groundwater levels with the Richards equation. *J. Hydrol.* 233 (1), 72–85.
- Van Der Walt, S., Colbert, S.C., Varoquaux, G., 2011. The NumPy array: a structure for efficient numerical computation. *Comput. Sci. Eng.* 13 (2), 22–30.
- Wang, J. et al., 2011. The coupled routing and excess storage (CREST) distributed hydrological model. *Hydrol. Sci. J.* 56 (1), 84–98.
- Wood, E.F., Lettenmaier, D.P., Zartarian, V.G., 1992. A land-surface hydrology parameterization with subgrid variability for general circulation models. *J. Geophys. Res. Atmos.* 97 (D3), 2717–2728.
- Xia, Y. et al., 2012a. Continental-scale water and energy flux analysis and validation for North American Land Data Assimilation System project phase 2 (NLDAS-2): 2. Validation of model-simulated streamflow. *J. Geophys. Res. Atmos.* 117 (D3).
- Xia, Y. et al., 2012b. Continental-scale water and energy flux analysis and validation for the North American Land Data Assimilation System project phase 2 (NLDAS-2): 1. Intercomparison and application of model products. *J. Geophys. Res. Atmos.* 117 (D3).
- Zhang, J. et al., 2016. Multi-Radar Multi-Sensor (MRMS) quantitative precipitation estimation: initial operating capabilities. *Bull. Am. Meteorol. Soc.* 97 (4), 621–638.
- Zhang, K., Kimball, J.S., Nemani, R.R., Running, S.W., 2010. A continuous satellite-derived global record of land surface evapotranspiration from 1983 to 2006. *Water Resour. Res.* 46 (9).
- Zhao, R.-J., 1992. The Xinanjiang model applied in China. *J. Hydrol.* 135 (1–4), 371–381.
- Zhao, R., Liu, X., 1995. The Xinanjiang model. In: Singh, V. (Ed.), *Computer Models of Watershed Hydrology*. Water Resources Publications, LLC, Littleton, Colorado, pp. 215–232.